

Shape, Shell Structure and Collective Modes Unique to Nuclei Far from Stability Line

Ikuko HAMAMOTO^{*)}

*Division of Mathematical Physics, LTH, University of Lund,
P. O. Box 118, S-22100 Lund, Sweden*

(Received December 29, 2001)

The structure of nuclei far from β -stability lines is expected to show various interesting and exotic phenomena, due to the unique features: (a) the presence of nucleons with very small binding energies and largely extended wave-functions; (b) large difference between the Fermi levels of protons and neutrons; (c) exotic ratios of the proton to neutron numbers for a given mass number. Among the topics, which are the direct consequence of those characteristic features and are being studied experimentally using the radioactive nuclear ion beam facilities in the world, I choose to talk about the one-particle shell-structure, response function, and related collective modes.

§1. Introduction

The magic numbers in nuclear physics, 2, 8, 20, 28, 50, 82, 126, \dots , are historically understood by approximating the mean-field potential of β -stable nuclei by the harmonic oscillator potential plus the spin-orbit potential. As the separation energy of nucleons decreases from 7–10 MeV in β -stable nuclei to nearly zero in drip line nuclei, the radial shape of the nuclear density and the resulting nuclear potential will deviate from that of the harmonic oscillator potential. Correspondingly, the nuclear shape and shell-structure including magic numbers can be changed. Moreover, the character of nuclear collective modes may also change as we approach drip lines, since the domination of quadrupole deformation in β -stable nuclei is due to ¹⁾ the similarity of the one-body potential of nuclei, which consist of a relatively small number of particles, to the harmonic oscillator potential.

It is experimentally known ^{2), 3)} that the nucleus $^{32}_{12}\text{Mg}_{20}$, which is a singly-closed-shell nucleus in the traditional sense, is deformed. In the present meeting we have heard the experimental observation of the change of magic numbers in very light nuclei far from the β stability line; $N = 8$ and $N = 20$ are no longer magic numbers in very neutron-rich nuclei. ⁴⁾ The appearance of a new magic number $N = 16$ in the neighborhood of the neutron drip line is suggested in Ref. ⁵⁾ analyzing the measured separation energies and interaction cross sections.

Examining the one-particle level structure of neutrons in the Woods-Saxon potential shown in Fig. 2-30 of Ref. 1), of which the potential parameters are appropriate for β -stable nuclei, it is already seen that $N = 28$ and $N = 50$ may not be magic numbers for neutrons with small binding energies. The disappearance of those magic numbers is made by filling in the one-particle energy-gaps at $N = 28$ and 50 by the $2p_{3/2}$ and $3s_{1/2}$ levels, respectively. In Fig. 1(a) we show the extension of

^{*)} E-mail: ikuko.hamamoto@matfys.lth.se

Fig. 2-30 of Ref. 1) to the region of small mass numbers, while in Fig. 1(b) energy eigenvalues of neutron orbitals are plotted for the Woods-Saxon potential with doubled diffuseness parameter, $a = 1.34$ fm, keeping all other parameters unchanged. From Figs. 1(a) and (b) it is seen that around $E_{n\ell j} = -10$ MeV, $N = 8$ and 20 are magic numbers as established in β -stable nuclei, while for neutron drip line nuclei $N = 16$ becomes a new magic number instead of $N = 8$ and 20. The change of the one-particle level structure for $E_{n\ell j} = -10 \rightarrow 0$ MeV originates from smaller values of the slope, $|dE_{n\ell j}/dA|$ for smaller ℓ orbitals as $|E_{n\ell j}|$ becomes smaller. Due to the lower centrifugal barrier the neutrons with smaller orbital angular momentum ℓ can easily extend their wave functions beyond the nucleus, as the binding energies decrease. For more diffuse potentials, which are appropriate for neutron-drip-line nuclei, the extension of one-particle wave-functions beyond the potential starts already at more strongly bound orbitals. In Ref. 6) the change of the shell structure in

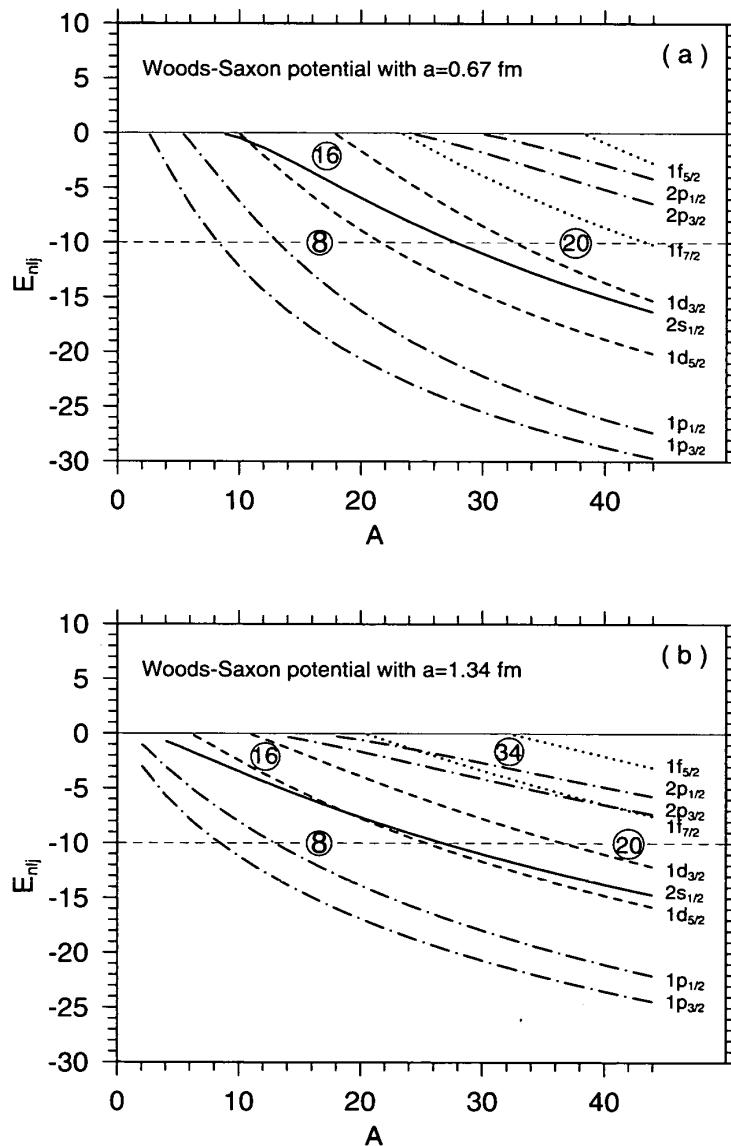


Fig. 1. Energies of neutron orbitals : (a) for the Woods-Saxon potential with standard parameters¹⁾ (b) the same as (a) except for the diffuseness parameter $a=1.34$ fm.

the neighborhood of the neutron drip line is analyzed in terms of two basic physics elements, kinetic energy and spin-orbit splitting.

As already stated above, around the neutron drip line the one-particle energy gap at $N = 50$ is expected to become small, since the neutron orbitals with smaller orbital angular momenta, especially the $3s_{1/2}$ and $2d_{5/2}$ orbitals, may energetically approach the lower-lying $1g_{9/2}$ orbital. Since the neutron drip line for $Z < 28$ may be reached in the present decade using RNB facilities currently planned, more information on the change of the shell structure in nuclei in the vicinity of the neutron drip line with $N \approx 60$ will become available in the near future. One way of detecting the disappearance of the large $N = 50$ energy gap is to examine the low-lying octupole collectivity of the nucleus ${}^{60}_{20}\text{Ca}_{40}$,⁷⁾ which may be more easily created in the laboratory in the near future. As ${}^{80}_{40}\text{Zr}_{40}$ is known to be most probably deformed, ${}^{60}_{20}\text{Ca}_{40}$ may be the heaviest (spherical) ℓ -s closed-shell nucleus, in which low-lying collective 2^+ states are absent. Performing constrained Hartree-Fock (HF) calculations with Skyrme interactions, it is indeed shown⁷⁾ that in ${}^{60}_{20}\text{Ca}_{40}$ there is no local HF energy minimum other than the one at spherical shape ($Q = 0$) and the calculated total energy increases steeply as $|Q|$ increases. Then, there is a good chance to observe collective octupole strength as low-lying threshold strength and, moreover, the octupole collectivity will depend very much on the one-particle energy-gap at $N = 50$.

In §2 two important elements in the change of nuclear shell-structure, one-particle kinetic energy and spin-orbit splitting, are discussed as a function of both orbital angular momentum ℓ and binding energy, when neutron binding energies decrease towards zero. In §3 the $N = 50$ energy gap estimated in the HF calculations is illustrated, and the low-lying octupole strength in ${}^{60}_{20}\text{Ca}_{40}$ is discussed in connection with the disappearance of the large $N = 50$ energy gap. Conclusions and further discussions are given in §4.

§2. One-particle kinetic energy and spin-orbit splitting⁶⁾

One-particle eigen-energy E_ν in the potential V is the sum of the positive kinetic energy $\langle \nu | T | \nu \rangle$ and the negative potential energy $\langle \nu | V | \nu \rangle$. For bound states, $E_\nu < 0$, the absolute magnitude of $\langle \nu | V | \nu \rangle$ is larger than $\langle \nu | T | \nu \rangle$. In the case of larger ℓ orbitals $|\langle \nu | V | \nu \rangle|$ becomes smaller while $\langle \nu | T | \nu \rangle$ gets larger, as $|E_\nu| \rightarrow 0$. In contrast, for smaller ℓ orbitals $\langle \nu | T | \nu \rangle$ does not become larger as $|E_\nu| \rightarrow 0$, since one-particle wave functions can extend beyond the potential due to lower centrifugal barriers. As a result of it, $|E_\nu|$ of smaller ℓ orbitals approaches very slowly towards zero, when the mass number A decreases (see Fig. 1).

The one-body potential in nuclei is written as

$$V(r) = U(r) + V_{\ell s}(r) + V_{\text{Coulomb}}(r), \quad (2.1)$$

where the nuclear one-body potential is expressed by $U(r)$. Using eigenfunctions with quantum numbers $(n\ell)$ in the absence of the Coulomb and spin-orbit potentials, the

Table I. Calculated quantities of one-particle ($n\ell$) neutron orbital in the finite square-well potential with radius R and depth U_0 , as the binding energy approaches zero. The probability of finding the particle inside the potential is given in the second column, while the quantity in the third column is proportional to the kinetic energy. The static E2 polarization charge, $e_{\text{pol}}(\text{E2})$, which is ¹⁾ proportional to the ratio of the quantity in the third column to that in the fourth column, is also shown in the fifth column.

ℓ	probability for $r \leq R$	$\langle \frac{r}{U_0} \frac{dU(r)}{dr} \rangle_{n\ell}$	$\langle r^2 \rangle_{n\ell}$	$e_{\text{pol}}(\text{E2})$
0	0	0	$\propto E_{n\ell} ^{-1} \Rightarrow \infty$	$\Rightarrow 0$
1	1/3	2/3	$\propto E_{n\ell} ^{-1/2} \Rightarrow \infty$	$\Rightarrow 0$
2	3/5	6/5	\Rightarrow finite	\Rightarrow small positive
3	5/7	10/7	\Rightarrow finite	\Rightarrow positive
↓	↓	↓		
∞	1	2		

expectation value of kinetic energy can be written as

$$\langle n\ell | T | n\ell \rangle = \frac{1}{2} \left\langle n\ell \left| r \frac{dU(r)}{dr} \right| n\ell \right\rangle \tag{2.2}$$

with a help of the virial theorem. It is interesting to note that the diagonal and nondiagonal matrix elements of the same operator, $r(dU(r)/dr)$, express the coupling to shape oscillations and thus are proportional to polarization charge. In a similar way we obtain

$$\text{spin-orbit splitting} \propto (2\ell + 1) \left\langle n\ell \left| \frac{1}{r} \frac{dU(r)}{dr} \right| n\ell \right\rangle \tag{2.3}$$

treating perturbatively the spin-orbit potential, of which the radial dependence is phenomenologically known as $(1/r)(dU(r)/dr)$.

First, in Table I we show various quantities for one-particle orbitals in the limit of zero binding-energy, which are calculated for finite square-well potentials with radius R and depth U_0 . Note that tabulated quantities are independent of the quantum number n and that the state $|n\ell\rangle$ is always an eigenstate of respective finite square-well potentials. It is seen from Table I that the kinetic energy of orbitals with smaller ℓ values decreases strongly as the binding energy decreases to zero. It can also be understood that in the same limit the spin-orbit splitting for smaller ℓ values decreases, though in a slightly milder way than the kinetic energy due to the different r -dependence of the relevant operators; $(1/r)(dU(r)/dr)$ vs $r(dU(r)/dr)$. See Ref. 6) for the detailed result of spin-orbit splitting. The extension of one-particle wavefunctions with small ℓ values beyond the potential is the origin of the decrease of kinetic energy as well as spin-orbit splitting, as the binding energies become smaller.

Next, we estimate at which binding energy for a given ℓ value the one-particle kinetic energy starts to decrease. In Fig. 2 the expectation values of the operator

$(r/U_0)(dU(r)/dr)$ for neutrons are shown for an infinite square-well potential, a finite square-well potential with the depth U_0 , and the Woods-Saxon potential with standard parameters with $U_0 = 50$ MeV and $N = Z$, as a function of $(1+(E_{n\ell}/U_0))$. For $U_0 = 50$ MeV $(1+(E_{n\ell}/U_0)) = 0.8$ and 1.0 mean $E_{n\ell} = -10$ and 0 MeV, respectively. Thus, the vertical dotted line at $(1+(E_{n\ell}/U_0)) = 0.8$ indicates the approximate position of the Fermi level of β -stable nuclei. In the infinite square-well potential ($U_0 \rightarrow \infty$), the kinetic energy is equal to $(U_0 + E_{n\ell})$ and, thus, the plotted quantity $(r/U_0)(dU(r)/dr)$ is equal to $2(1+(E_{n\ell}/U_0))$ for all orbitals independent of $(n\ell)$ values. In other words, one-particle wave-functions cannot extend beyond

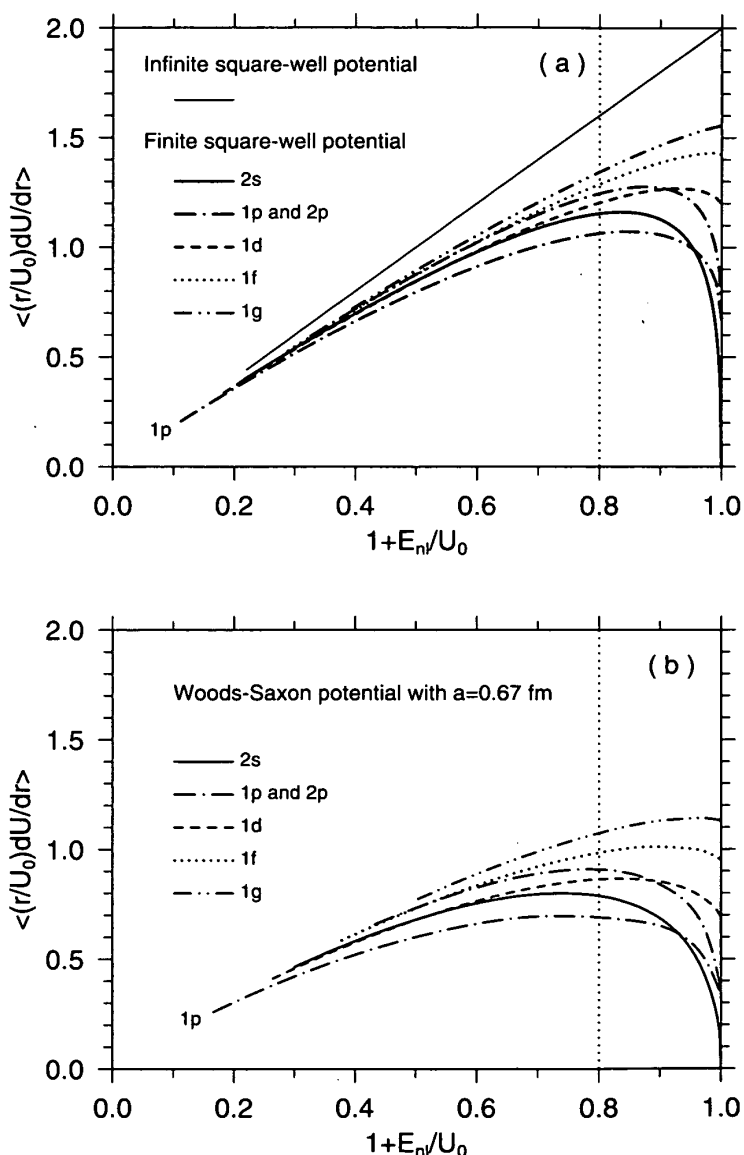


Fig. 2. Expectation values of the dimensionless quantity, $(r/U_0)(dU(r)/dr)$, which are proportional to kinetic energy of respective one-particle orbitals, as a function of $(1+(E_{n\ell}/U_0))$. For $U_0=50$ MeV $(1+(E_{n\ell}/U_0))=0.8$ and 1.0 mean $E_{n\ell} = -10$ and 0 MeV, respectively. Figures are taken from Ref. 6). (a) For the square-well potential with the depth U_0 . For the infinite square-well potential, the thin straight line is common for all orbitals with various (n, ℓ) values; (b) for the Woods-Saxon potential with standard parameters.¹⁾ The figure is taken from Ref. 6).

the potential and, thus, the reduction in the increasing rate of kinetic energy never occurs, as $(1+(E_{n\ell}/U_0))$ increases. For the Woods-Saxon potential with standard parameters¹⁾ the kinetic energy of orbitals with smaller ℓ values starts to decrease around $E_{n\ell} \approx -10$ MeV, as seen from Fig. 2(b). It is seen that for less diffuse potentials and for larger ℓ orbitals a considerable deviation from the straight line occurs first at smaller values of binding energies. For example, as seen from Fig. 2(a), for the finite square-well potential the plotted quantity for the 1g orbital is almost a straight line up till zero binding energy, and even for $\ell=0$ orbitals it starts to decrease first at very small binding energies.

§3. Low-lying collective octupole strength in ${}^{60}_{20}\text{Ca}_{40}$ ⁷⁾

In Fig. 3 we show the HF single-particle energy levels together with the HF potentials, which are calculated for ${}^{60}_{20}\text{Ca}_{40}$ using a spherical HF code with the SkM* interaction. It is seen that the $Z = 50$ energy gap is 5.52 MeV, while the $N = 50$ energy gap, namely the energy distance between the $1g_{9/2}$ neutron level and the $2d_{5/2}$ one-neutron resonant level is only 1.97 MeV. Moreover, the virtual (i.e., the phase shift does not pass through $\pi/2$) $3s_{1/2}$ level is in fact located below the $2d_{5/2}$ resonant level in the continuum. We note that in two other $N = 40$ nuclei, ${}^{68}_{28}\text{Ni}_{40}$ and ${}^{80}_{40}\text{Zr}_{40}$, which lie away from the neutron drip line, the $N = 50$ energy gap estimated in the same HF code is 4.48 and 5.32 MeV and, furthermore, the $3s_{1/2}$ level lies higher than the $2d_{5/2}$ level by 0.98 and 2.00 MeV, respectively.

In Fig. 4(a) we show the low-energy part of the calculated octupole strength of the isoscalar (IS) RPA and that of the unperturbed neutron excitations to the continuum in ${}^{60}_{20}\text{Ca}_{40}$. The response function is obtained by using the self-consistent HF calculation plus RPA with SkM* interaction performed in coordinate space. In Fig. 4(b) the unperturbed strengths obtained by exciting neutrons from individual occupied orbitals to the continuum are shown. The strength summed over all unperturbed neutron strengths in Fig. 4(b) is plotted as the dotted curve in Fig. 4(a). There are four (two proton and two neutron) unperturbed excitations from bound to bound states, which are not plotted in Fig. 4(b) since the dimension of the strengths is different. The contributions by these four unperturbed strengths are not included in the dotted curve in Fig. 4(a), however, they naturally appear in the RPA strength due to the coupling to the continuum states.

The calculated threshold energy is 3.41 MeV, which is the binding energy of the $1f_{5/2}$ neutrons. For the excitation of neutrons in the $1f_{5/2}$ orbitals indicated by the dashed curve in Fig. 4(b), the lowest peak at 3.45 MeV comes from the $\ell=0$ threshold strength (or possibly the excitation to the virtual $3s_{1/2}$ state), while the peaks around 4.04, 5.3 and 9.5 MeV come from the excitations to the one-particle resonant $2d_{5/2}$ state, to the broad distribution of the virtual $2d_{3/2}$ state and to the one-particle resonant $1g_{7/2}$ state, respectively. For the excitation of neutrons in the $2p_{1/2}$ orbital shown by the solid curve, the excitations to the $\ell=0$ states as well as to the virtual $2d_{3/2}$ state are absent, while the peaks around 5.6 and 11.0 MeV come from the excitations to the one-particle-resonant $2d_{5/2}$ and $1g_{7/2}$ states, respectively. In this way, it is understood that the appearance of the low-energy neutron octupole

excitations in the continuum is created by the disappearance of the large $N = 50$ energy gap. Below the threshold one RPA state (not shown in Fig. 4(a)) is obtained at $E_x = 1.92$ MeV, which originates from the neutron excitation, $1f_{5/2} \rightarrow 1g_{9/2}$, and is not very collective. The downward shifting of the peak energies in RPA is due to the attractive nature of the IS RPA correlation. From Fig. 4(a) it is fairly clear that three peaks of the enhanced IS RPA strength at $E_x < 5$ MeV originate from the three peaks of the dotted curve at 3.44, 4.04 and 5.61 MeV. If the energy distance between the $1g_{9/2}$ and $(2d_{5/2})_{\text{res}}$ levels (or the virtual $3s_{1/2}$ level) were much larger, say 5 MeV, the low-lying collective RPA octupole strength would have been pushed up by 3 MeV.

According to our experience in very light nuclei, HF calculations with available

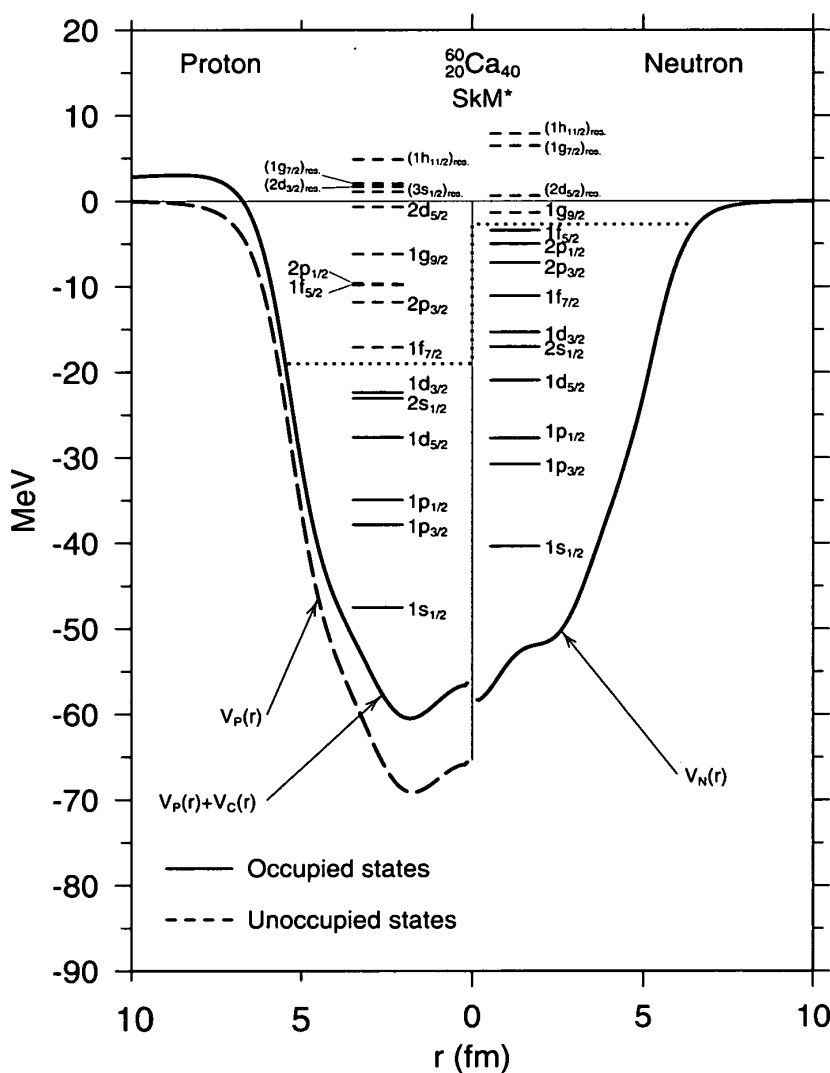


Fig. 3. Hartree-Fock potentials and one-particle energy levels for the nucleus $^{60}_{20}\text{Ca}_{40}$, which are calculated with the SkM* interaction, neutrons on the r.h.s. and protons on the l.h.s. $V_N(r)$ expresses the neutron nuclear potential, while $V_P(r)$ and $V_C(r)$ denote the proton nuclear and Coulomb potentials, respectively. The notation $(nlj)_{\text{res}}$ expresses the calculated one-particle resonant levels in the HF potential, for which the phase shifts pass through $\pi/2$. Occupied levels are indicated by full lines, while unoccupied levels are denoted by broken lines. The dotted line shows an approximate position of the Fermi level.

Skyrme interactions are known to produce too many nuclei lying inside the neutron drip line. For example, though both ${}^{28}_8\text{O}_{20}$ and ${}^{26}_8\text{O}_{18}$ are experimentally known to lie beyond the neutron drip line, almost all HF calculations available predict these nuclei to be stable against neutron emission. Examining the systematics of the measured neutron separation energy, one may expect that $1g_{9/2}$ neutron level of ${}^{60}_{20}\text{Ca}_{40}$ should have been in the continuum, while it is obtained as a bound level in our calculation. If the $1g_{9/2}$ level is unbound, there may be no bound neutron-excitations and a stronger octupole strength may appear as threshold strength. Though the lowest-lying negative-parity state of ${}^{60}_{20}\text{Ca}_{40}$ may happen to be a 5^- state, the high-multipole state is very unlikely to be a collective state.

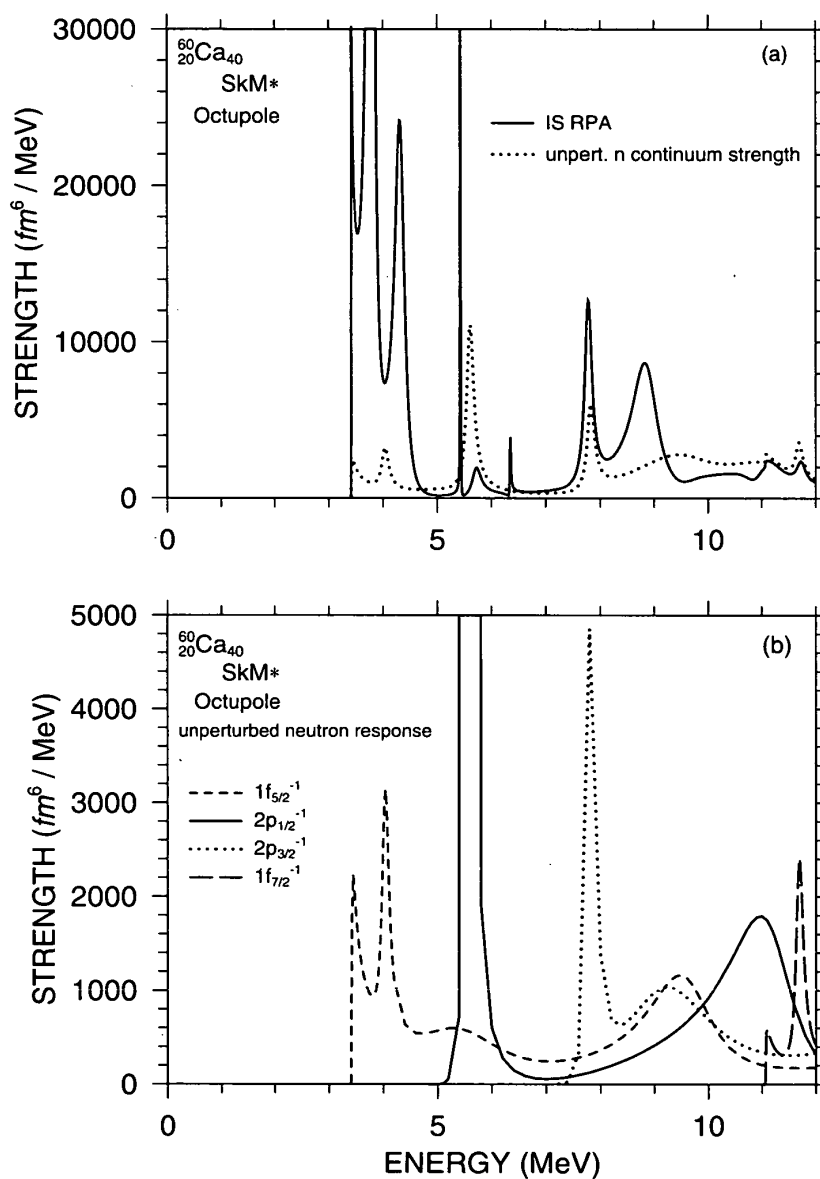


Fig. 4. (a) Comparison of the low-lying octupole strength of the IS RPA with that of the unperturbed neutron excitation to the continuum. (b) Unperturbed octupole strength obtained by exciting neutrons from occupied given orbitals to the continuum. The figure is taken from Ref. 7).

§4. Conclusions and discussion

When neutron one-particle energies vary as $E_{nlj} = -10 \rightarrow 0$ MeV, we have shown that the shell structure can be considerably changed because both one-particle kinetic energy and spin-orbit splitting decrease more strongly for small ℓ orbitals and, moreover, the decrease is stronger for more diffuse potentials. It is also shown that kinetic energy is more sensitive to the diffuse surface of potentials than spin-orbit splitting. Our finding of the variation of both kinetic energy and spin-orbit splitting explains the change of the observed shell-structure that around the neutron drip line the traditional magic numbers $N = 8$ and 20 disappear while a new magic number $N = 16$ appears. In shell model calculations of drip line nuclei one must properly take into account those basic elements in the change of shell structure.

In the present meeting T. Otsuka has stated⁸⁾ that the result of his shell model calculations shows the appearance of new magic numbers $N = 16$ and $N = 34$ due to the attractive neutron-proton interaction in the $(\vec{\sigma} \cdot \vec{\sigma})(\vec{\tau} \cdot \vec{\tau})$ channel. Since the harmonic oscillator wave-functions are used in the shell-model calculations, the effect of small binding energies of one-particle orbitals on the nuclear shell-structure, which is discussed in §2, is absent in the calculation of Ref. 8). Nevertheless, it is interesting to notice that the new magic numbers $N=16$ and $N=34$ discussed in Ref. 8) happen to coincide with those which are obtained from Fig. 1. In fact, it has been known already for years (for example, Refs. 9) and 10)) that the attractive short-range neutron-proton interaction can push down particular neutron (proton) one-particle levels as protons (neutrons) start to occupy relevant orbitals. As a result of it, the shell structure can be changed. A typical example known in the sixties¹⁰⁾ is that the spin-parity of the ground state of ${}_{51}\text{Sb}$ isotopes changes from $5/2^+$ to $7/2^+$ for $N \geq 72$ as the neutrons start to occupy the $1h_{11/2}$ orbital, due to the large overlap of the wave functions of the proton $1g_{7/2}$ and neutron $1h_{11/2}$ orbitals. In order to change the shell structure due to the attractive neutron-proton interaction, it is not very clear to us whether or not the interaction in the $(\vec{\sigma} \cdot \vec{\sigma})(\vec{\tau} \cdot \vec{\tau})$ channel is more important than that in the $(\vec{\tau} \cdot \vec{\tau})$ channel. In the Skyrme HF calculations the interaction strength in the $(\vec{\sigma} \cdot \vec{\sigma})(\vec{\tau} \cdot \vec{\tau})$ channel, which does not contribute to the present HF result, is very poorly determined. On the other hand, to reproduce the observed values of total binding energies and nuclear radii, etc., is fully taken care of by the interaction in the $(\vec{\tau} \cdot \vec{\tau})$ channel. Thus, we can safely conclude that in our HF calculations both the effect of the attractive neutron-proton interaction and that of the small binding energies of one-particle orbitals are included in the obtained shell structure.

Close to the neutron drip line the neutron number $N = 50$ is expected to be no longer a magic number. The disappearance of the magic number $N = 50$ may be exhibited by the low-lying collective octupole strength of the nucleus ${}_{20}^{60}\text{Ca}_{40}$, which is predicted to be spherical and rigid against quadrupole deformation. This is an interesting case that the low-lying octupole threshold strength may be very collective. The low-lying, strongly collective octupole strength should be alternatively detected by a large renormalization of the one-particle octupole moment (due to the polarization of the core) in the neighboring odd-A nuclei.

Acknowledgements

The author is grateful to Crafoordska stiftelsen for a financial support for the present research.

References

- 1) A. Bohr and B. R. Mottelson, *Nuclear Structure* (Benjamin, Reading, MA, 1975), vol. II.
- 2) D. Guillemaud-Mueller et al., *Nucl. Phys. A* **426** (1984), 37.
- 3) T. Motobayashi et al., *Phys. Lett. B* **346** (1955), 9.
- 4) H. Sakurai, *Prog. Theor. Phys. Suppl. No. 146* (2002), 39.
- 5) A. Ozawa et al., *Phys. Rev. Lett.* **84** (2000), 5493.
- 6) I. Hamamoto, S. Lukyanov and X. Z. Zhang, *Nucl. Phys. A* **683** (2001), 255.
- 7) I. Hamamoto, H. Sagawa and X. Z. Zhang, *Phys. Rev. C* **64** (2001), 024313.
- 8) T. Otsuka, *Prog. Theor. Phys. Suppl. No. 146* (2002), 6.
- 9) L. S. Kisslinger and R. A. Sorensen, *Rev. Mod. Phys.* **35** (1963), 853.
- 10) I. Hamamoto, *Nucl. Phys.* **86** (1966), 208.